JOURNAL OF COMPUTATIONAL PHYSICS 92, 313–348 (1991)

# Multigrid Methods for Two- and Three-Dimensional Poisson-Type Equations on the Sphere

SAULO R. M. BARROS*

*Gesellschaft für Mathematik und Datenverarbeitung, D5205 St. Augustin 1, Federal Republic of Germany*

Received June 6, 1989; revised October 25, 1989

The efficient solution of two- and three-dimensional Poisson- and Helmholtz-type equations on the sphere with multigrid methods is the subject of this work. The strong anisotropic behavior of the Laplacian in spherical coordinates poses severe requirements on the relaxation procedures, in order to attain a full multigrid effectiveness. The introduction of a new technique, *combined relaxation*, results in high efficiency, even in cases with varying anisotropy direction, where alternating line or plane relaxations would normally be required. The combination of this new relaxation technique with semi-coarsening strategies is also studied. Even for moderate grid sizes, the multigrid solvers developed are shown to be competitive with two-dimensional, direct fast solvers, in cases where the latter can be applied. The optimal computational complexity of the multigrid methods, their broad applicability (in contrast to fast direct solvers), and their high efficiency, also in three spatial dimensions, make these methods very interesting for applications. 

## INTRODUCTION

The solution of elliptic equations in spherical geometries is of interest for many applications, for example, in astro- and geophysics. We describe in this work the development of efficient multigrid solvers for two- and three-dimensional Poisson- and Helmholtz-type equations on the sphere. The crucial problems one has to deal with when solving these equations are the singularities and the strong anisotropy of the Laplacian in spherical coordinates. These problems lead to the requirement for special multigrid components, without which one would be far away from reaching the full efficiency of the method.

The treatment of singularities already begins with the discretization, since the Laplacian in spherical coordinates is not formally defined there. Through the use of finite volume techniques, a discrete equation is naturally derived at these points. In addition to that, the obtained second-order discretization is conservative and can be symmetrized easily. This property also allows for the analytic derivation of discrete compatibility conditions for the Poisson equation in the sphere (with pure Neumann boundary conditions) and on the surface of a sphere. These conditions

* Current address: Instituto de Matematica e Estatistica, University of Sao Paulo, Caixa Postal 20570, Brazil.



0021-9991/91 $3.00

(analogous to the continuous ones) must be satisfied in order to ensure that the discrete set of equation possesses a solution.

An essential part of the multigrid method is the process of error-smoothing, since (only) a smoothed error can be well approximated on a coarser grid. For isotropic problems one can normally achieve a good smoothing by using standard (suitable) pointwise relaxation procedures (like Gauss–Seidel, SOR, etc.). It is well known that this is no longer true if the problem is anisotropic, for which more sophisticated relaxation methods (such as line, or even plane, relaxation for some 3D problems) are required (e.g., [7, 13, 15]).

The elliptic problems in spherical coordinates treated here are all highly anisotropic. Depending on the mesh size relations, the anisotropy even changes its direction inside the domain, leading to poor smoothing properties of usual line (or plane in 3D) relaxations. Expensive alternating line (plane) relaxations should then be used (cf., [7, 13]).

Instead of using these alternating-type relaxation methods, we propose a new technique, *combined relaxation*. In this procedure, the domain is subdivided according to a local Fourier analysis, so that in each subdomain the anisotropy direction remains unchanged. The relaxation to be used in each subdomain is then chosen according to the local anisotropy direction. In two dimensions, the obtained relaxation is as cheap as a usual line relaxation and has very good smoothing properties. The same idea is extended to three dimensions and, although with a more involved implementation, since it requires plane relaxation, also gives significant improvements. Similar ideas about exploiting the local behaviour of the equations were proposed in early works by Brandt [6] in the so-called "local relaxation sweeps." There, however, an arbitrary subdivision of the domain was suggested (in an adaptive procedure).

As an alternative in the treatment of anisotropies in three-dimensional problems, we investigate the use of semi-coarsening (e.g., [13]), which should be useful in order to avoid plane relaxation. We discuss the difficulties of using this technique for varying anisotropy, where the anisotropy direction on coarser grids can change, even if it does not change on the finest one. As a consequence, the behavior of the multigrid method deteriorates. We show then how to combine semi-coarsening and line relaxation on fine grids with standard coarsening and plane relaxation on coarser grids in order to overcome these problems. With this combination, plane relaxation (at least) on the finest grid is avoided and efficiency is improved.

The performance of the developed multigrid methods can be observed through the presented numerical results. In order to get an impression of the efficiency, we also made comparative tests with the well-known (based on Buneman's reduction method) direct fast solver of FISHPAK [1], for the 2D Poisson equation on the surface of a sphere. Both methods are comparable for medium-sized problems, while the better complexity of the multigrid method (with a computational work proportional to the number of unknowns) leads to a better performance of this method on finer grids. Another point is that, in contrast to the restricted applicability of fast direct solvers, the multigrid method can be used in more general situations (e.g., for the Helmholtz-type equations in [4, 5]) and, as we show in this work, is extendable (maintaining efficiency) to 3D problems in spherical coordinates. (No special assumptions are made in the three-dimensional case. For the special situation of axisymmetry, when the problem can be reduced to two dimensions, an efficient multigrid method has been presented in [11].)

Throughout this paper we assume that the reader is familiar with multigrid terminology. For those who are not, we refer to [7, 10, 13], where complete descriptions of the method and its variants can be found. The paper is divided as follows. A description of the discretization used is given in Section 1. Section 2 is dedicated to problems on the surface of a sphere. The combined relaxation is introduced in this section. The three-dimensional problem is treated in Section 3. We first analyze the use of standard coarsening techniques and show the necessity for using plane relaxation. The extension of combined relaxation to three dimensions is described and a number of numerical experiments are presented. Semi-coarsening strategies are also discussed. Concluding remarks are given in Section 4.

## 1. Discretization

We derive in this section a discretization for the Poisson equation on the sphere:

$$\Delta u = f \qquad \text{in} \quad \Omega = \{(x, y, z) \colon x^2 + y^2 + z^2 < 1\},$$

with Neumann boundary conditions

$$\frac{\partial u}{\partial \mathbf{n}} = g \qquad \text{in} \quad \partial\Omega.$$

A discretization for the Poisson equation (with periodic boundary conditions) on the surface of the sphere will also be obtained.

We apply the orthogonal transformation

$$\Phi = \begin{pmatrix} x(r, \phi, \theta) = r \sin\phi \cos\theta \\ y(r, \phi, \theta) = r \sin\phi \sin\theta \\ z(r, \phi, \theta) = r \cos\phi \end{pmatrix}$$

to map the region $\Omega^* = \{(r, \phi, \theta)\colon 0 \leqslant r \leqslant 1,\ 0 \leqslant \phi \leqslant \pi,\ 0 \leqslant \theta \leqslant 2\pi\}$ onto the unit sphere. See Fig. 1.

The transformed Laplacian is written in spherical coordinates as:

$$\Delta = \frac{1}{r^2}\frac{\partial}{\partial r}\left(r^2 \frac{\partial}{\partial r}\right) + \frac{1}{r^2 \sin\phi}\frac{\partial}{\partial \phi}\left(\sin\phi \frac{\partial}{\partial \phi}\right) + \frac{1}{r^2 \sin^2\phi}\frac{\partial^2}{\partial \theta^2}. \tag{1.1}$$

For the equation on the surface of the sphere, we set $r = 1$ and eliminate the first term in the expression for the Laplacian (the region $\Omega^*$ becomes two-dimensional).

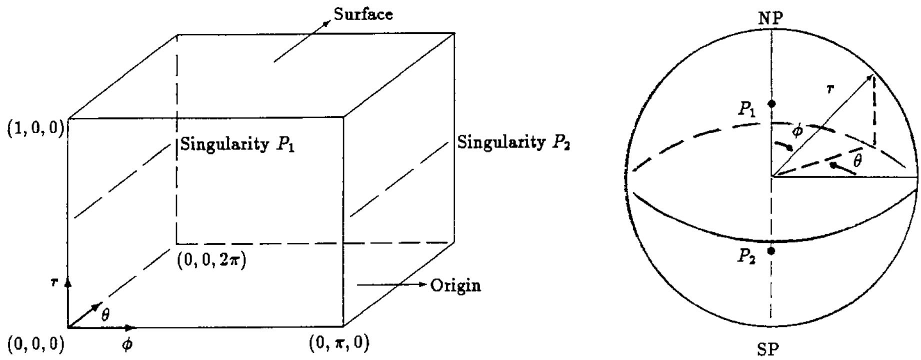


FIG. 1. Computational and physical domains.

For the full sphere, the following computational grid is defined in $\Omega^*$,

$$G_h^* = \{(r_i, \phi_j, \theta_k): i=0, ..., N_r, j=0, ..., N_\phi, k=0, ..., N_\theta\}, \tag{1.2}$$

with $r_i = ih_r$, $\phi_j = jh_\phi$, $\theta_k = kh_\theta$, and where the mesh sizes are given by $h_r = 1/N_r$, $h_\phi = \pi/N_\phi$, and $h_\theta = 2\pi/N_\theta$. The quantities $N_r$, $N_\phi$, and $N_\theta$ are chosen, in order to allow usual coarsening strategies, as powers of two or as small prime numbers (3 or 5) times a power of two. The computational grid on the surface of the sphere is obtained through the restriciton $r=1$. We remark that to each singularity (where the determinant of the Jacobian of the transformation vanishes) there corresponds a whole line or plane in the computational domain. Points corresponding to a singularity are then naturally identified (see Fig. 1).

In order to obtain a finite volume discretization, we divide the computational domain into control volumes (cells), each of them corresponding to a grid point $(r_i, \phi_j, \theta_k)$:

$$\Omega^*_{i,j,k} := \left(\left[r_i - \frac{h_r}{2}, r_i + \frac{h_r}{2}\right] \times \left[\phi_j - \frac{h_\phi}{2}, \phi_j + \frac{h_\phi}{2}\right] \times \left[\theta_k - \frac{h_\theta}{2}, \theta_k + \frac{h_\theta}{2}\right]\right) \cap \bar{\Omega}^*. \tag{1.3}$$

See Fig. 2. The cell faces are denoted, for example, as:

$$\Gamma^*_{i\pm 1/2,j,k} = r_i \pm \frac{h_r}{2} \times \left[\phi_j - \frac{h_\phi}{2}, \phi_j + \frac{h_\phi}{2}\right] \times \left[\theta_k - \frac{h_\theta}{2}, \theta_k + \frac{h_\theta}{2}\right]. \tag{1.4}$$

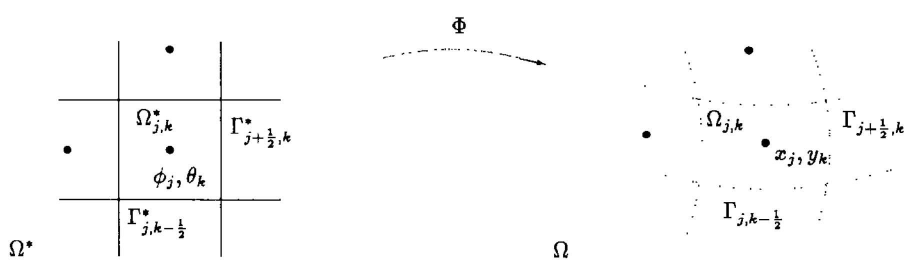


FIG. 2. Control volumes and their faces.

The faces $\Gamma^*_{i,j\pm 1/2,k}$ and $\Gamma^*_{i,j,k\pm 1/2}$ are defined similarly. (Near the boundary of $\Omega^*$ we have half cells, quarter cells, ....) In an analogous way we define the cells in the two-dimensional case (on the surface of the sphere). Through the mapping $\Phi$ we obtain the "physical" (on the sphere) grid $G_h = \Phi(G_h^*)$, cells ($\Omega_{i,j,k} = \Phi(\Omega^*_{i,j,k})$), and their faces. This transformation is sketched in 2D in Fig. 2.

*Remark.* The smaller cells $\Omega^*_{i,j,0}$ and $\Omega^*_{i,j,N_\theta}$ actually correspond to the same physical grid point (due to the periodicity in the $\theta$-coordinate). These cells are then joined to form just one cell around this grid point.

We now derive the discrete equations at nonsingular points. For the sake of simplicity we restrict the description to two dimensions (on the surface of the sphere). At a point $(\phi_j, \theta_k)$ (with $1 \leqslant j \leqslant N_\phi - 1$ and $1 \leqslant k \leqslant N_\theta$, see remark above for $k = N_\theta$), we integrate

$$\Delta u = \nabla \cdot \nabla u = f$$

over the corresponding control volume. By the divergence theorem, one obtains

$$\int_{\Omega_{j,k}} \Delta u = \int_{\partial\Omega_{j,k}} \nabla u \cdot \mathbf{n} = \int_{\Omega_{j,k}} f,$$

with $\mathbf{n}$ denoting the outward unity normal vector. Using the inverse of the mapping $\Phi$ and its orthogonality, we have

$$\int_{\Omega_{j,k}} \Delta u = \int_{\Gamma^*_{j+1/2,k}} \sin\phi \frac{\partial u}{\partial\phi} - \int_{\Gamma^*_{j-1/2,k}} \sin\phi \frac{\partial u}{\partial\phi} + \int_{\Gamma^*_{j,k+1/2}} \frac{1}{\sin\phi} \frac{\partial u}{\partial\theta} - \int_{\Gamma^*_{j,k-1/2}} \frac{1}{\sin\phi} \frac{\partial u}{\partial\theta}.$$

Each of the line integrals is then approximated by the midpoint rule and the derivatives involved on it by central differences. For example,

$$\int_{\Gamma^*_{j+1/2,k}} \sin\phi \frac{\partial u}{\partial\phi} = h_\theta \sin\phi_{j+1/2} \frac{u(\phi_{j+1}, \theta_k) - u(\phi_j, \theta_k)}{h_\phi}.$$

The integration of the right-hand side $f$ is also accomplished through the midpoint rule,

$$\int_{\Omega_{j,k}} f = f(\phi_j, \theta_k) V_{j,k},$$

where $V_{j,k} = h_\theta h_\phi \sin\phi_j$ approximates the volume of the cell. We obtain all together the five-point star,

$$\left[\frac{h_\theta}{h_\phi} \sin\phi_{j-1/2} \quad -\sum_{h_\phi/(h_\theta \sin\phi_j)}^{h_\phi/(h_\theta \sin\phi_j)} \quad \frac{h_\theta}{h_\phi} \sin\phi_{j+1/2}\right] u_{j,k} = h_\theta h_\phi \sin\phi_j f_{j,k}, \tag{1.5}$$

where $\sum$ denotes the sum of the four neighbours.

We come now to the treatment of the singularities. To each of them correspond more than one point on the computational domain, which must be identified. The integration of the equation is now performed over all corresponding cells at once. At the north pole $P_N$ (where $\phi = 0$) we obtain (with the definition $\Omega_0 = \Phi(\bigcup_{k=0}^{N_\theta} \Omega^*_{0,k})$),

$$\int_{\Omega_0} \Delta u = \sum_{k=0}^{N_\theta} \int_{\Omega_{0,k}} \Delta u = \sum_{k=1}^{N_\theta} h_\theta \sin \phi_{1/2} \frac{u(\phi_1, \theta_k) - u(P_N)}{h_\phi},$$

where we again use the midpoint rule in the line integrals and central differences to approximate derivatives. The periodicity in the $\theta$-coordinate was also used to join the two quarter cells $\Omega_{0,0}$ and $\Omega_{0,N_\theta}$ into a half cell like the others. By discretizing the right-hand side as

$$\int_{\Omega_0} f = f(P_N)\, V_N = f(P_N)\, \pi \frac{h_\phi}{2} \sin \phi_{1/2}$$

we obtain

$$\sum_{k=1}^{N_\theta} \frac{h_\theta}{h_\phi} \sin \phi_{1/2}(u(\phi_1, \theta_k) - u(P_N)) = f(P_N)\, \pi \frac{h_\phi}{2} \sin \phi_{1/2} = f(P_N)\, V_N. \tag{1.6}$$

Analogously, at the south pole one obtains

$$\sum_{k=1}^{N_\theta} \frac{h_\theta}{h_\phi} \sin \phi_{N_\phi - 1/2}(u(\phi_{N_\phi - 1}, \theta_k) - u(P_S))$$
$$= f(P_S)\, \pi \frac{h_\phi}{2} \sin \phi_{N_\phi - 1/2} = f(P_S)\, V_S. \tag{1.7}$$

There are several important remarks to be made:

(a) Integrals on faces common to two cells are approximated in the same way by the discretization in each of them. This is important for obtaining a conservative discretization. Another consequence is that the final discretization on the surface of the sphere is symmetric.

(b) At nonsingular grid points, the discretization is virtually identical to a central difference discretization (up to a multiplicative factor, which depends on the grid point being considered). However, central differences cannot be directly applied to discretize the equation at singularities.

(c) The last remark already shows that the discretization is second order at nonsingular points. It is easily shown by Taylor's expansions that second order is also achieved at the poles.

(d) In order that the Poisson equation has a solution on the surface of the sphere, the right-hand side $f$ has to satisfy the compatibility condition $\int_\Omega f = 0$. The solution is then unique just up to a constant. The discrete equation preserves these properties. The symmetry of the discretization is quite useful in deriving the discrete compatibility condition that must be fulfilled. Since in each discrete equation the sum of the coefficients equals zero, the constant function belongs to the kernel of the discretization matrix. By elimination of one row and one column of this matrix. a diagonally dominant and irreducible matrix is obtained and, therefore, the constant function spans the kernel of the discretization matrix. This shows that the discrete solution is unique up to a constant, when it exists. In order for a solution to exist, the discrete right-hand side has to be orthogonal (in the Euclidian inner product) to the kernel of the adjoint of the discretization matrix. Due to the symmetry of the matrix, the constant function also spans this kernel. The compatibility condition then just says that the sum of all right-hand sides have to be zero. This means that $\sum f_{j,k} V_{j,k} = 0$, which is a second-order approximation to the continuous compatibility condition $\int_\Omega f = \sum \int_{\Omega_{i,k}} f = 0$.

(e) Normally, the discrete compatibility condition will note be fulfilled, even when the continuous condition is. The right-hand side must then be modified in order to ensure the existence of a solution to the discrete problem. With $F_{j,k} = f_{j,k} V_{j,k}$ we have the following compatibility condition: $\langle F, \mathbf{1} \rangle = 0$ (which will normally be satisfied only up to an $O(h^2)$ term). By modifying $F$ as $\bar{F} = F - (\langle F, \mathbf{1} \rangle / \langle v, \mathbf{1} \rangle) v$ (with any function $v$), one will obtain the fulfilment of the condition. One has, however, to be careful of the choice of $v$, in order not to destroy the order of accuracy. Concentrating the correction on just one grid point, for example, would lead to inconsistency of the discretization there. Two possible choices are to take $v \equiv \mathbf{1}$ or $v_{i,j} = V_{i,j}$, which would correspond to changes of order $O(h^2)$ in $f$ at each point, keeping the discretization second order. Our choice will be $v_{i,j} = V_{i,j}$, equivalent to the addition of a constant to the right-hand side $f$.

(f) The discretization (1.5)–(1.7) has already been used in [14] (with (1.5) in finite difference form). The discrete compatibility condition and the necessity of modifying the right-hand side in order to obtain a solution were also discussed there. However, the order of consistency of the discretization and the influences of the perturbation of the right-hand side on it were not analyzed in that work. We include here the whole derivation of the discretization in order to consider it within the framework of finite volumes, which furnish a simple way of treating the singularities and of achieving a conservative, symmetric second-order discretization. The treatment of compatibility conditions is also trivial in this framework. The same techniques are applied in three dimensions; it is merely for convenience that we present a detailed description only in two dimensions.

We come now to the three-dimensional discretization on the sphere, which is also obtained by finite volume techniques as in the two-dimensional case. At a non-singular point $(r_i, \phi_j, \theta_k)$ we get the seven-point star,

$$\left[\frac{A_\theta}{\sin\phi_j}\left[A_\phi \sin\phi_{j-1/2} \quad -\sum_{A_r \sin\phi_j r_{i-1/2}^2}^{A_r \sin\phi_j r_{i+1/2}^2} \quad A_\phi \sin\phi_{j+1/2}\right]_\phi^r \frac{A_\theta}{\sin\phi_{j\theta}}\right]_\theta u_{i,j,k}$$
$$= f_{i,j,k} r_i^2 \sin\phi_j h_\phi h_r h_\theta, \tag{1.8}$$

where $A_\theta = h_\phi h_r / h_\theta$, $A_\phi = h_\theta h_r / h_\phi$, $A_r = h_\theta h_\phi / h_r$, and $\sum$ denotes the sum of the neighbours. One obtains at inner points on the north pole–south pole axis $P_i = (r_i, \phi, \theta)$ (with $\phi = 0$ or $\phi = \pi$),

$$\frac{\pi h_\phi}{2h_r} \sin \frac{h_\phi}{2} \left(r_{i+1/2}^2 (u(P_{i+1}) - u(P_i)) + r_{i-1/2}^2 (u(P_{i-1}) - u(P_i))\right)$$
$$+ A_\phi \sin \frac{h_\phi}{2} \sum_{k=1}^{N_\theta} (u(r_i, \bar{\phi}, \theta_k) - u(P_i))$$
$$= \frac{1}{2} f(P_i)\, \pi r_i^2 h_r h_\phi \sin \frac{h_\phi}{2}, \tag{1.9}$$

where $\bar{\phi} = h_\phi$ (if $\phi = 0$) or $\bar{\phi} = \pi - h_\phi$ (if $\phi = \pi$). At the origin $P_0 = (0, 0, 0)$, we obtain

$$\frac{A_r h_r^2}{4} \sum_{k=1}^{N_\theta} \sum_{j=1}^{N_\phi - 1} \sin \phi_j (u(r_1, \phi_j, \theta_k) - u(P_0))$$
$$+ \frac{\pi h_r h_\phi}{8} (u(r_1, 0, 0) - 2u(P_0) + u(r_1, \pi, 0))$$
$$= f(P_0) \frac{\pi h_\phi h_r^3 S}{12}, \tag{1.10}$$

where $S = \sin h_\phi/2/2 + \sum_{j=1}^{N_\phi - 1} \sin \phi_j$. At nonsingular boundary points one obtains $P = (1, \phi_j, \theta_k)$,

$$\left[\frac{A_\theta}{\sin \phi_j} \left[A_\phi \sin \phi_{j-1/2} \quad \underset{A_r \sin \phi_j ((1 - h_r/2)^2 + (1 + h_r/2)^2)}{-\sum} \quad A_\phi \sin \phi_{j+1/2}\right]_\phi^r \frac{A_\theta}{\sin \phi_j}\right]_\theta u_{i,j,k}$$
$$= f_{i,j,k} \sin \phi_j h_\phi h_r h_\theta - 2h_r A_r \sin \phi_j (1 + h_r/2)^2 g_{i,j,k} \tag{1.11}$$

and at the poles $P_{N_r} = (1, \phi, \theta)$ (with $\phi = 0$ or $\phi = \pi$),

$$\frac{\pi h_\phi}{2h_r} \sin \frac{h_\phi}{2} \left(\left(1 - \frac{h_r}{2}\right)^2 + \left(1 + \frac{h_r}{2}\right)^2\right) (u(P_{N_r - 1}) - u(P_{N_r}))$$
$$+ A_\phi \sin \frac{h_\phi}{2} \sum_{k=1}^{N_\theta} (u(1, \bar{\phi}, \theta_k) - u(P_{N_r}))$$
$$= \frac{1}{2} f(P_{N_r})\, \pi h_r h_\phi \sin \frac{h_\phi}{2} - 2h_r \frac{\pi h_\phi}{2h_r} \sin \frac{h_\phi}{2} (1 + h_r/2)^2 g(P_{N_r}), \tag{1.12}$$

where $\bar{\phi} = h_\phi$ (if $\phi = 0$) or $\bar{\phi} = \pi - h_\phi$ (if $\phi = \pi$).

In the discretization at boundary points we have already incorporated the boundary conditions. An extension of the control volumes to the outside of the domain was used to obtain a discrete equation like (1.8). It involves, however, a (ghost) point outside the domain. In the usual way of treating Neumann boundary conditions, the outer normal derivatives (in the $r$-direction) were approximated through central differences. At a point $P=(1, \phi_j, \theta_k)$ the approximation is

$$\frac{\partial u}{\partial \mathbf{n}}=\frac{u(1+h_r, \phi_j, \theta_k)-u(1-h_r, \phi_j, \theta_k)}{2h_r}=g(P).$$

The expression obtained for the ghost point, $u(1+h_r, \phi_j, \theta_k)=u(1-h_r, \phi_j, \theta_k)+2h_r g(P)$, is then substituted in the equation at the boundary, leading to (1.11). Discretization (1.12) is obtained analogously, departing from a discretization like (1.9).

The final discretization has at every point the order of consistency two. This is proved again by using Taylor's expansions [3].

We point out that the final discretization is not symmetric, due to the treatment of the boundary conditions. It can, however, be easily symmetrized by multiplying each equation at boundary points by $(1-h_r/2)^2/((1-h_r/2)^2+(1+h_r/2)^2)$. The new discretization matrix is then symmetric and the considerations about compatibility conditions from the two-dimensional case are still valid. In particular, it becomes trivial to obtain the discrete compatibility condition, which is now a second-order approximation to the continuous one $\int_\Omega f-\int_{\partial\Omega} g=0$ (see [3] for a proof).

Once the complete discretization is obtained, one can use an equivalent formulation of it, such as the finite difference form at nonsingular points (obtained from the finite volume discretization through division by the approximated cell volumes). This actually has the effect of destroying the symmetry of the discretization, but this is not important for methods such as multigrid (for some other methods one would naturally prefer the symmetric form). In our multigrid solvers we are actually going to use an equivalent formulation of the equations, obtained by scaling each equation as follows. On the surface of the sphere we multiply

$$(1.5) \text{ by } \frac{h_\phi}{h_\theta \sin\phi_j}, \qquad (1.6) \text{ and } (1.7) \text{ by } \frac{2h_\phi}{\pi \sin h_\phi/2}, \tag{1.13}$$

and in the three-dimensional case we multiply

$$\begin{gathered}(1.8) \text{ and } (1.11) \text{ by } \frac{h_\phi}{h_\theta h_r \sin\phi_j}, \qquad (1.10) \text{ by } \frac{12}{h_r h_\phi \pi S}, \\ (1.9) \text{ and } (1.12) \text{ by } \frac{2h_\phi}{\pi h_r \sin h_\phi/2}.\end{gathered} \tag{1.14}$$

## 2. Multigrid Methods on the Surface of a Sphere

We present in this section a multigrid solver for a model elliptic equation on the surface of the sphere, the Poisson equation with periodic boundary conditions. This solver can be easily adapted to treat other Poisson-type problems, such as the Helmholtz equations treated in Section 3.4.

The Poisson equation is discretized according to (1.5)–(1.7) and (1.13), including the perturbation of the right-hand side in order to satisfy the discrete compatibility condition (see remark (a) in Section 1). The discrete solution (in agreement with the [illegible] constructed as follows:

(a) *Grids and coarsening.* The finest grid is defined by (1.2) (restricted to the surface of the sphere), while the coarser grids are obtained by successively doubling the meshsizes of the finest grid (standard coarsening, e.g., [13]). The coarse grid operators are defined in the same way as on the finest grid.

(b) *Transfer operators.* Residuals are transfered from finer to coarser grids by a (transformed) full-weighting operator (e.g., [7]). At nonsingular grid points it is defined by the star (with $(\phi_j, \theta_k)$ denoting the corresponding fine-grid point at which the transfer takes place):

$$\frac{1}{4}\begin{bmatrix} \dfrac{\sin\phi_{j-1}}{\sin\phi_j} & 2 & \dfrac{\sin\phi_{j+1}}{\sin\phi_j} \\ 2\dfrac{\sin\phi_{j-1}}{\sin\phi_j} & 4 & 2\dfrac{\sin\phi_{j+1}}{\sin\phi_j} \\ \dfrac{\sin\phi_{j-1}}{\sin\phi_j} & 2 & \dfrac{\sin\phi_{j+1}}{\sin\phi_j} \end{bmatrix}. \tag{2.1}$$

At the poles we need a special definition of this operator. It is derived in such a way, that the transferred residuals will automatically satisfy the discrete compatibility condition on the coarse grid, once the corresponding condition on the fine grid is fulfilled. Denoting by $R$ the residual function on the fine grid, the transferred residual at a pole $P$ is defined as

$$2\frac{\sin(h_\phi/2)}{\sin h_\phi} R(P) + \frac{4}{N_\theta}\sum_{k=1}^{N_\theta} R(\bar{\phi}, \theta_k), \tag{2.2}$$

where $\bar{\phi} = h_\phi$ (if $\phi = 0$) or $\bar{\phi} = \pi - h_\phi$ (if $\phi = \pi$). $N_\theta$ is the number of grid points on the fine grid in the $\theta$-direction. This is an average of all residuals surrounding the pole. Bilinear interpolation is employed to transfer the corrections from coarser to finer grids.

(c) *Relaxation.* Having made the choice to use standard coarsening, we need to find a relaxation procedure, which should rapidly reduce the high-frequency components of the error function (related to a given approximation to the solution) in all grid directions. Due to the strong anisotropy of the Laplacian in spherical coordinates, especially near the poles where its coefficients in the $\theta$-direction are orders of magnitude greater than in the $\phi$-direction, usual pointwise relaxation methods will have poor smoothing properties. Line relaxation methods should be used in these circumstances (e.g., [13]).

A local mode analysis can provide qualitative and quantitative information about given relaxation procedures [7]. Through the smoothing factor $\mu(\nu)$ one can predict the behavior of a multigrid method, which employs $\nu$ sweeps of the corresponding relaxation in each multigrid cycle. One can roughly expect an overall reduction of the error after each multigrid cycle by a factor of about $\mu(\nu)^{\nu}$ (for small values of $\nu$). This smoothing analysis (for problems with variable coefficients) is performed at all grid points. Actually, the operator is frozen at each point and an idealized constant-coefficient problem on an infinite grid is analysed instead. A coupling between low and high harmonics (caused by some relaxations, such as red–black and zebra-line) is taken into account by the simulation of a multigrid cycle, which employs an ideal coarse grid correction operator, which annihilates all low frequencies and does not affect high-frequency Fourier components. We refer to [13] for a detailed description of the local analysis.

Now we present results of a smoothing analysis for some point and line relaxation methods. Other versions of these relaxations (with different ordering of grid points) have qualitatively similar properties to the corresponding versions treated here. For all versions considered we have for the local smoothing factor,

$$\mu(\nu, p) = \sup_{-\pi/2 < \Theta \leqslant \pi/2} \left\{ \sqrt[\nu]{\frac{|A_1^{2\nu-1}(1-A_1)|}{2}}, |A_2|^2 \right\}, \qquad p \in G_h^{*,0}, \tag{2.3}$$

where $G_h^{*,0}$ denotes the interior of $G_h^*$. In particular, the poles and the boundaries are not considered in the analysis. The global smoothing factor $\mu(\nu)$ is obtained by taking the supremum over all local smoothing factors. The values $A_1$ and $A_2$ depend on the grid point $(\phi_j, \theta_k)$ and on the frequency $\Theta = (\Theta_1, \Theta_2)$. They take the following values for:

*point red–black relaxation*:

$$A_1(\Theta) = \frac{\cos\dfrac{h_\phi}{2}\cos\Theta_2 + \dfrac{q_l^2}{\sin^2\phi}\cos\Theta_1 + i\dfrac{\cos\phi}{\sin\phi}\sin\dfrac{h_\phi}{2}\sin\Theta_2}{\cos\dfrac{h_\phi}{2} + \dfrac{q_l^2}{\sin^2\phi}} \tag{2.4}$$

$$A_2(\Theta) = A_1(\Theta_1 + \pi, \Theta_2);$$

*θ-zebra line relaxation*:

$$A_1(\Theta) = \frac{\cos\dfrac{h_\phi}{2}\cos\Theta_2 + i\dfrac{\cos\phi}{\sin\phi}\sin\dfrac{h_\phi}{2}\sin\Theta_2}{\cos\dfrac{h_\phi}{2} + \dfrac{q_l^2}{\sin^2\phi}(1-\cos\Theta_1)} \tag{2.5}$$

$$A_2(\Theta) = A_1(\Theta_1 + \pi, \Theta_2);$$

*$\phi$-zebra line relaxation*:

$$A_1(\Theta) = \frac{\dfrac{q_l^2}{\sin^2\phi}\cos\Theta_1}{\dfrac{q_l^2}{\sin^2\phi} + \cos\dfrac{h_\phi}{2}(1-\cos\Theta_2) + i\dfrac{\cos\phi}{\sin\phi}\sin\dfrac{h_\phi}{2}\sin\Theta_2} \tag{2.6}$$

$$A_2(\Theta) = A_1(\Theta_1, \Theta_2 + \pi).$$

The value

$$q_l = h_\phi / h_\theta \tag{2.7}$$

describes the meshsize ratio. Equations (2.3), (2.4), and (2.6) show that red–black and $\phi$-zebra relaxation give a poor global smoothing. The smoothing factors approach unity for points near the poles. On the other hand, it can be seen that $\theta$-zebra line relaxation smooths very well if $q_l \geqslant 1$. In this case we obtain $\mu(2) \leqslant 0.34$ and can expect convergence factors around 0.1 for multigrid cycles employing two sweeps of relaxation on each grid level. For smaller values of $q_l$ we get a more complicated picture, since then there is a change in the anisotropy direction inside the domain and none of the relaxations considered have good smoothing factors. An alternating line relaxation (with a sweep of line relaxation in one direction followed by one in the other direction) would be necessary to provide the required smoothing [7, 13]. Tables I–IV contain the asymptotic convergence factors for

TABLE I

$V(1, 1)$ Multigrid Convergence Factors with Line Relaxations when $q_l = 2$

| | Relaxation | |
|---|---|---|
| $N_\theta, N_\phi$ | $\theta$-Line | $\phi$-Line |
| 32, 8 | 0.020 | 0.76 |
| 64, 16 | 0.030 | 0.93 |
| 128, 32 | 0.040 | 0.97 |
| 256, 64 | 0.045 | 0.98 |

TABLE II

$V(1, 1)$ Multigrid Convergence Factors with Line Relaxations when $q_l = 1$

| | Relaxation | |
|---|---|---|
| $N_\theta, N_\phi$ | $\theta$-Line | $\phi$-Line |
| 32, 16 | 0.042 | 0.76 |
| 64, 32 | 0.054 | 0.93 |
| 128, 64 | 0.059 | 0.97 |
| 256, 128 | 0.063 | 0.98 |

TABLE III

$V(1, 1)$ Multigrid Convergence Factors with Line Relaxations when $q_l = 0.5$

| $N_\theta, N_\varphi$ | Relaxation: $\theta$-Line | $\varphi$-Line | Altern. line |
|---|---|---|---|
| 16, 16 | 0.31 | 0.63 | 0.031 |
| 32, 32 | 0.36 | 0.76 | 0.031 |
| 64, 64 | 0.39 | 0.93 | 0.040 |
| 128, 128 | 0.41 | 0.97 | 0.047 |

TABLE IV

$V(1, 1)$ Multigrid Convergence Factors with Line Relaxations when $q_l = 0.25$

| $N_\theta, N_\phi$ | Relaxation: $\theta$-Line | $\phi$-Line | Altern. line |
|---|---|---|---|
| 8, 16 | 0.68 | 0.34 | 0.026 |
| 16, 32 | 0.72 | 0.53 | 0.031 |
| 32, 64 | 0.75 | 0.76 | 0.042 |
| 64, 128 | 0.77 | 0.93 | 0.051 |

$V(1, 1)$-cycles with various relaxations for several situations. They are in agreement with the results of the smoothing analysis.

## 2.1. *Combined Relaxation*

It was shown in the last section, by a mode analysis and numerical experiments, that the single line relaxation methods were not sufficient for very good multigrid convergence factors in cases with $q_l < 1$. There is actually no sudden deterioration of the convergence factors when crossing the point $q_l = 1$, but they will gradually get worse with smaller values of $q_l$. (However, for $q_l < 1$ it starts to be more effective to apply line relaxation in the other direction, in some parts of the domain.) In these cases, $\theta$-line relaxation smooths well near the poles but can not provide a good smoothing near the equator, where the anisotropy has another direction. Only with an alternating line relaxation, where $\phi$-line relaxation accounts for the good smoothing in the region (near the equator) where $\theta$-line relaxation does not perform well and vice versa, are typically good multigrid convergence factors achieved. The major inconvenience of alternating line relaxation is its cost; it requires twice the computational work of a single line relaxation.

In order to overcome these deficiencies, we have developed the combined relaxation method, which explores the local information available. The idea is to choose the relaxation in a determined region according to the local behavior of the discrete

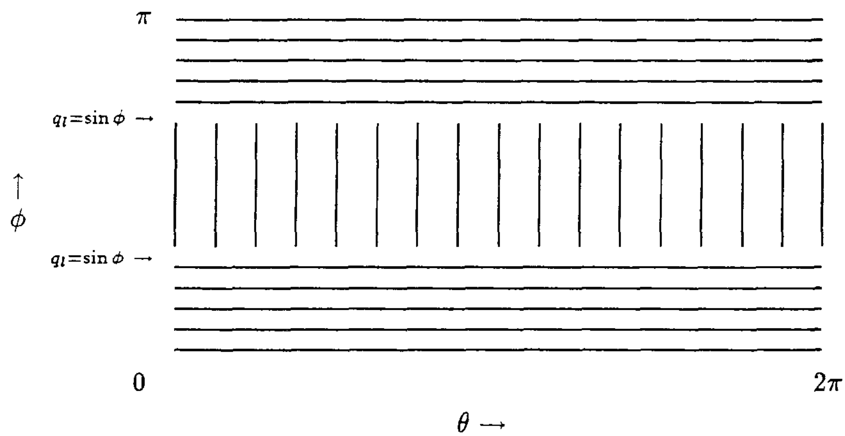


FIG. 3. Pattern of the combined relaxation for cases with $q_l < 1$.

operator. In order to do this, we need to split the domain into disjoint regions such that the anisotropy has a fixed direction inside each. In other words, we want to apply each line relaxation only in the region in which it smooths very well. The choice of the appropriate splitting to use is made with the aid of local mode analysis. According to (2.3), (2.5), and (2.6), $\theta$-line relaxation does an excellent job (with $\mu(2) \approx 0.3$) in regions where $q_l \geqslant \sin\phi$, while $\phi$-line relaxation is the most effective where $q_l < \sin\phi$. We then split the domain into regions according to whether $q_l \geqslant \sin\phi$ or otherwise. The pattern of the combined relaxation is illustrated in Fig. 3.

The practical implementation of combined relaxation is done as follows. First we perform $\theta$-line relaxation zebrawise (odd lines first, then even lines) on the regions around the poles (where $q_l \geqslant \sin\phi$). Then we apply $\phi$-zebra line relaxation near the equator (where $q_l < \sin\phi$). We note taht the tridiagonal systems now involved in the relaxation for the $\phi$-direction are smaller than the original ones, due to the

TABLE V

$V(1, 1)$ Multigrid Convergence Factors with the Combined and with the Alternating Line Relaxation

| $q_l = 0.5$ | | | $q_l = 0.25$ | | |
|---|---|---|---|---|---|
| | Relaxation | | | Relaxation | |
| $N_\theta, N_\phi$ | Altern. | Combin. | $N_\theta, N_\phi$ | Altern. | Combin. |
| 16, 16 | 0.031 | 0.044 | 8, 16 | 0.026 | 0.026 |
| 32, 32 | 0.031 | 0.054 | 16, 32 | 0.031 | 0.059 |

TABLE VII

Comparative Results between the Multigrid Solver and FISHPAK for Grids with Mesh Size Relation $q_l = 1.0$

| | Full multigrid | | FISHPAK | |
|---|---|---|---|---|
| $N_\theta, N_\phi$ | Error | CPU time | Error | CPU time |
| 32, 16 | 7.88-03 | 10 | 8.00-03 | 10 |
| 64, 32 | 2.04-03 | 33 | 2.00-03 | 33 |
| 128, 64 | 5.12-04 | 119 | 4.99-04 | 136 |
| 256, 128 | 1.28-04 | 453 | 1.25-04 | 590 |

*Note.* Errors in the uniform norm and CPU times (in milliseconds) necessary for solving the equation are presented.

For the sake of comparison we also show results (including CPU times) obtained with the direct fast solver from FISHPAK [1], which is based on reduction methods. We can conclude that the multigrid solver is competitive with the direct fast solver, even in cases with varying anisotropy directions ($q_l = 0.5$). For very fine grids the multigrid solver compares even better, since it has a superior time complexity to that of the direct solver from FISHPAK ($O(N_\theta N_\phi)$ against $O(N_\theta N_\phi \log N_\theta)$) (see Tables VII and VIII).

We point out that the multigrid solver presented here has a more general use than just for the Poisson equation. Its adaption to more general Helmholtz and Helmholtz-type equations is straightforward, with little change to the components of the solver. We use it here, for example, to solve the Helmholtz equations related to $(\phi, \theta)$-plane relaxations, which are used for the 3D Poisson equation (see Section 3). A multigrid method using staggered grids in the solution of similar equations appearing in meteorological models was described in [4]. Another application in meteorology is presented in [5].

TABLE VIII

Comparative Results between the Multigrid Solver and FISHPAK for Grids with Mesh Size Relation $q_l = 0.5$

| | Full multigrid | | FISHPAK | |
|---|---|---|---|---|
| $N_\theta, N_\phi$ | Error | CPU time | Error | CPU time |
| 16, 16 | 2.19-02 | 10 | 2.02-02 | 3 |
| 32, 32 | 5.36-03 | 23 | 5.27-03 | 13 |
| 64, 64 | 1.33-03 | 70 | 1.33-03 | 63 |
| 128, 128 | 3.33-04 | 243 | 3.33-04 | 263 |

*Note.* Errors in the uniform norm and CPU times (in milliseconds) necessary for solving the equation are presented.

## 3. The Three-Dimensional Poisson Equation on the Sphere

We consider now the three-dimensional Poisson equation with Neumann boundary conditions on the unit sphere. The equation is discretized as described in Section 1 according to (1.8)–(1.12) and (1.14). We again enforce the right-hand side to fulfil the compatibility condition according to remark (e) of Section 1. We start by developing multigrid methods in connection with the standard coarsening strategy. These methods will also be of importance when examining the alternative semi-coarsening in Section 3.7.

### 3.1. *Multigrid Components for Standard Coarsening*

Our finest grid is defined by (1.2); the coarser grids (constructed by standard coarsening) have the same structure. In order to transfer residuals from finer to coarser grids, a (transformed) full-weighting operator is applied. With this transformed operator the geometry of the sphere is taken into account and the resulting operator has variable coefficients. It is given

at non-singular points $(r, \phi, \theta)$ by the 27-point star,

$$\frac{1}{16}\underbrace{\begin{bmatrix} \frac{\sin(\phi-h_\phi)}{\sin\phi} & 2 & \frac{\sin(\phi+h_\phi)}{\sin\phi} \\ 2\frac{\sin(\phi-h_\phi)}{\sin\phi} & 4 & 2\frac{\sin(\phi+h_\phi)}{\sin\phi} \\ \frac{\sin(\phi-h_\phi)}{\sin\phi} & 2 & \frac{\sin(\phi+h_\phi)}{\sin\phi} \end{bmatrix}_\phi^r}_{\theta-h_\theta \text{ and } \theta+h_\theta} \underbrace{\begin{bmatrix} 2\frac{\sin(\phi-h_\phi)}{\sin\phi} & 4 & 2\frac{\sin(\phi+h_\phi)}{\sin\phi} \\ 4\frac{\sin(\phi-h_\phi)}{\sin\phi} & 8 & 4\frac{\sin(\phi+h_\phi)}{\sin\phi} \\ 2\frac{\sin(\phi-h_\phi)}{\sin\phi} & 4 & 2\frac{\sin(\phi+h_\phi)}{\sin\phi} \end{bmatrix}_\phi^r}_{\theta} : \tag{3.1}$$

at interior singularities on the polar axis $(r, \phi, \theta)$ by

$$\frac{2}{N_\theta}\sum_{k=1}^{N_\theta}(R(r, \bar{\phi}, kh_\theta) + (R(r+h_r, \bar{\phi}, kh_\theta) + R(r-h_r, \bar{\phi}, kh_\theta))/2)$$
$$+\frac{\sin(h_\phi/2)}{\sin(h_\phi)}(R(r, \phi, \theta) + (R(r+h_r, \phi, \theta) + R(r-h_r, \phi, \theta))/2), \tag{3.2}$$

with $\bar{\phi}$ as in (2.2) and $R$ the residual function on the fine grid;

at the origin by

$$\frac{S(h_\phi)}{4S(2h_\phi)}R(0,0,0) + \frac{3}{S(2h_\phi)h_\phi^2}\left(\frac{\sin(h_\phi/2)}{4}(R(h_r,0,0) + R(h_r,\pi,0))\right.$$
$$\left.+\sum_{j=1}^{N_\phi-1}\sin(jh_\phi)\frac{1}{N_\theta}\sum_{k=1}^{N_\theta}R(h_r, jh_\phi, kh_\theta)\right), \tag{3.3}$$

with $S = S(h_\phi) = 0.5 \sin(h_\phi/2) + \sum_{j=1}^{N_\phi - 1} \sin(jh_\phi)$, with $h_\phi$ from the fine grid and $R$ as in 3.2;

at nonsingular points $(1, \phi, \theta)$ on the boundary by

$$\frac{1}{16} \underbrace{\begin{bmatrix} 2\dfrac{\sin(\phi - h_\phi)}{\sin\phi} & 4 & 2\dfrac{\sin(\phi + h_\phi)}{\sin\phi} \\ 2\dfrac{\sin(\phi - h_\phi)}{\sin\phi} & 4 & 2\dfrac{\sin(\phi + h_\phi)}{\sin\phi} \end{bmatrix}_\phi^r}_{\theta - h_\theta \text{ and } \theta + h_\theta} \underbrace{\begin{bmatrix} 4\dfrac{\sin(\phi - h_\phi)}{\sin\phi} & 8 & 4\dfrac{\sin(\phi + h_\phi)}{\sin\phi} \\ 4\dfrac{\sin(\phi - h_\phi)}{\sin\phi} & 8 & 4\dfrac{\sin(\phi + h_\phi)}{\sin\phi} \end{bmatrix}_\phi^r}_{\theta}; \tag{3.4}$$

and at singularities $(1, \phi, \theta)$ on the boundary by

$$\frac{2}{N_\theta} \sum_{k=1}^{N_\theta} (R(1, \bar{\phi}, kh_\theta) + R(1 - h_r, \bar{\phi}, kh_\theta)) + \frac{\sin(h_\phi/2)}{\sin(h_\phi)} (R(1, \phi, \theta) + R(1 - h_r, \phi, \theta)). \tag{3.5}$$

The interpolation of corrections from coarser to finer grids is performed with the aid of trilinear interpolation.

### 3.2. *The Necessity for Plane Relaxations*

When applying standard coarsening we need a relaxation procedure with good smoothing properties in all grid directions. For Poisson-type problems with uniform Cartesian grids, the usual point Gauss–Seidel relaxation has the desired properties, while two-dimensional anisotropic problems require line relaxations. However, none of these techniques provides a good smoothing in our case. The anisotropy we have to deal with is caused by the spherical grid. The coefficients of the transformed Laplacian differ by orders of magnitude in each coordinate direction, especially near the singularities. This makes it necessary to use plane relaxation in order to efficiently damp the high frequencies of the error (see [6]). A plane relaxation is a block relaxation, where one has to solve simultaneously for all unknowns belonging to the same grid plane. Therefore, each sweep of this relaxation requires the solution of a series of two-dimensional problems. The efficiency in solving these problems is crucial for the feasibility of the plane relaxation and consequently of the whole method. It is a natural idea to apply multigrid also to the solution of these 2D problems [6]. In [15], this idea was systematically investigated for anisotropic model operators of the type

$$au_{xx} + bu_{yy} + cu_{zz},$$

with positive constants $a$, $b$, and $c$. Ideal combinations of multigrid components for different values of a, b, and c are summarized in [15]. Important for efficiency was the realization that only an approximate solution of the 2D problems (through just

TABLE IX

[illegible]

| Case | Coarsening | Relaxation |
|---|---|---|
| $a \approx b \approx c$ | Standard | Point |
| $a \approx b \ll c$ | Standard | $z$-line |
| $a \ll b \approx c$ | Standard | $(y, z)$-plane |
| | $(y, z)$-semi | Point |
| $a \ll b \ll c$ | Standard | $(y, z)$-plane |
| | $(y, z)$-semi | $z$-line |

one multigrid cycle on each plane) is required for smoothing. We repeat some results from [15] in Table IX.

When treating the Laplacian in spherical coordinates; we have to deal with variable coefficients; to get any insight into our problem from the results in Table IX, we need to freeze the coefficients. Points near the singularities relate to the last row in Table IX, which suggests the necessity of using $(\phi, \theta)$-plane relaxation in connection with standard coarsening. The next section provides a more careful analysis of this observation.

### 3.3. *Smoothing Analysis*

As in the two-dimensional case, the relaxations examined here couple Fourier harmonics. The effect of a given relaxation on high frequencies is therefore analyzed with the aid of an ideal two-grid operator, which employs this relaxation. Details about how to perform the analysis are given in [3]. We consider a red–black $\theta$-line relaxation (where lines are arranged in a red–black order) and plane relaxations in different directions. The analysis of the line relaxation (in the direction of the stronger couplings, as normally recommended) is included to illustrate why line relaxations do not smooth well in this case. Besides that, it will be useful when considering semi-coarsening strategies. We obtain (analogously to (2.3)) the following local smoothing factors:

$$\mu(\nu, p) = \sup_{-\pi/2 < \Theta \leqslant \pi/2} \left\{ \sqrt[\nu]{\frac{|A_1^{2\nu-1}(1-A_1)|}{2}}, |A_2|^2, |A_3|^2, |A_4|^2 \right\}, \qquad p \in G_h^{*,0}, \qquad (3.6)$$

where $G_h^{*,0}$ denotes the interior of $G_h^*$ (singularities and boundary points are not considered in the analysis). $A_1$ to $A_4$ are functions of $\Theta = (\Theta_1, \Theta_2, \Theta_3)$ and of $p = (r, \phi, \theta)$. They assume the following values in case of

*red–black $\theta$-line relaxation*

$$A_1(\Theta) = \frac{q^2\left(r^2 + \frac{h_r^2}{4}\right)\cos\Theta_1 + \cos\frac{h_\phi}{2}\cos\Theta_2 + i\left(q^2 r h_r \sin\Theta_1 + \frac{\cos\phi}{\sin\phi}\sin\frac{h_\phi}{2}\sin\Theta_2\right)}{q^2\left(r^2 + \frac{h_r^2}{4}\right) + \cos\frac{h_\phi}{2} + \frac{q_l^2}{\sin^2\phi}(1 - \cos\Theta_3)}$$

$$\begin{aligned} A_2(\Theta) &= A_1(\Theta_1, \Theta_2, \Theta_3 + \pi) \\ A_3(\Theta) &= A_1(\Theta_1, \Theta_2 + \pi, \Theta_3) \\ A_4(\Theta) &= A_1(\Theta_1, \Theta_2 + \pi, \Theta_3 + \pi) \end{aligned} \tag{3.7}$$

*$(\phi, \theta)$-zebra plane relaxation*

$$\begin{aligned} A_1(\Theta) &= \frac{q^2\left(r^2 + \frac{h_r^2}{4}\right)\cos\Theta_1 + iq^2 r h_r \sin\Theta_1}{q^2\left(r^2 + \frac{h_r^2}{4}\right) + \cos\frac{h_\phi}{2}(1-\cos\Theta_2) + \frac{q_l^2}{\sin^2\phi}(1-\cos\Theta_3) - i\frac{\cos\phi}{\sin\phi}\sin\frac{h_\phi}{2}\sin\Theta_2} \\ A_2(\Theta) &= A_1(\Theta_1, \Theta_2, \Theta_3 + \pi) \\ A_3(\Theta) &= A_1(\Theta_1, \Theta_2 + \pi, \Theta_3) \\ A_4(\Theta) &= A_1(\Theta_1, \Theta_2 + \pi, \Theta_3 + \pi) \end{aligned} \tag{3.8}$$

*$(r, \theta)$-zebra plane relaxation*

$$\begin{aligned} A_1(\Theta) &= \frac{\cos\frac{h_\phi}{2}\cos\Theta_2 + i\frac{\cos\phi}{\sin\phi}\sin\frac{h_\phi}{2}\sin\Theta_2}{\cos\frac{h_\phi}{2} + q^2\left(r^2 + \frac{h_r^2}{4}\right)(1-\cos\Theta_1) + \frac{q_l^2}{\sin^2\phi}(1-\cos\Theta_3) - iq^2 r h_r \sin\Theta_1} \\ A_2(\Theta) &= A_1(\Theta_1, \Theta_2, \Theta_3 + \pi) \\ A_3(\Theta) &= A_1(\Theta_1 + \pi, \Theta_2, \Theta_3) \\ A_4(\Theta) &= A_1(\Theta_1 + \pi, \Theta_2, \Theta_3 + \pi) \end{aligned} \tag{3.9}$$

*$(r, \phi)$-zebra plane relaxation*

$$\begin{aligned} A_1(\Theta) &= \frac{\frac{q_l^2}{\sin^2\phi}\cos\Theta_3}{\frac{q_l^2}{\sin^2\phi} + q^2\left(r^2 + \frac{h_r^2}{4}\right)(1-\cos\Theta_1) + \cos\frac{h_\phi}{2}(1-\cos\Theta_2) - iI} \\ A_2(\Theta) &= A_1(\Theta_1 + \pi, \Theta_2, \Theta_3) \\ A_3(\Theta) &= A_1(\Theta_1, \Theta_2 + \pi, \Theta_3) \end{aligned} \tag{3.10}$$

[redacted] $q_l$ are given by

$$q = h_\phi / h_r \qquad \text{and} \qquad q_l = h_\phi / h_\theta. \tag{3.11}$$

In order to see that the $\theta$-line relaxation smooths poorly, it is enough to substitute $\Theta = (\pi/2, 0, 0)$ in the expression for $A_3$ in (3.7), which will approach unity for $p$ near the origin, and use (3.6). By taking the same value of $\Theta$ and points near the origin and making use of (3.6), (3.9), and (3.10), one derives that neither the $(r, \theta)$- nor the $(r, \phi)$-plane relaxation smooths well.

Consider now the $(\phi, \theta)$-plane relaxation, which according to the simple considerations from the last section should be suitable for this problem. By neglecting the imaginary parts in the the expressions for $A_1$ to $A_4$ in (3.8) (which should be reasonable, at least for grid points that are not very close to the singularities) and calling the new quantities $\bar{A}_1$ to $\bar{A}_4$, we obtain that

$$\bar{A}_1(\Theta) = \frac{q^2\left(r^2 + \dfrac{h_r^2}{4}\right)\cos\Theta_1}{q^2\left(r^2 + \dfrac{h_r^2}{4}\right) + \cos\dfrac{h_\phi}{2}(1 - \cos\Theta_2) + \dfrac{q_l^2}{\sin^2\phi}(1 - \cos\Theta_3)}$$

varies between 0 and 1, and consequently,

$$\sup_{p \in G_h^*} \sup_{-\pi/2 < \Theta \leqslant \pi/2} \left\{ \sqrt[\nu]{\frac{|\bar{A}_1^{2\nu-1}(1-\bar{A}_1)|}{2}} = \left(\frac{2\nu-1}{2\nu}\right)^2 \Big/ \sqrt[\nu]{2(2\nu-1)} = \begin{cases} 0.125, & \nu = 1 \\ 0.23, & \nu = 2. \\ 0.32, & \nu = 3 \end{cases} \right.$$

For the other terms we obtain

$$\sup_{-\pi/2 < \Theta \leqslant \pi/2} |\bar{A}_2| = \frac{q^2(r^2 + h_r^2/4)}{q^2(r^2 + h_r^2/4) + q_l^2/\sin^2\phi}, \tag{3.12}$$

$$\sup_{-\pi/2 < \Theta \leqslant \pi/2} |\bar{A}_3| = \frac{q^2(r^2 + h_r^2/4)}{q^2(r^2 + h_r^2/4) + \cos h_\phi/2}, \tag{3.13}$$

and $|\bar{A}_4| \leqslant |\bar{A}_2|$, $|\bar{A}_4| \leqslant |\bar{A}_3|$. At every grid point, where

$$q^2(r^2 + h_r^2/4) \leqslant q_l^2/\sin^2\phi \qquad \text{and} \qquad q^2(r^2 + h_r^2/4) \leqslant \cos(h_\phi/2), \tag{3.14}$$

we have $|\bar{A}_2| \leqslant 0.5$ and $|\bar{A}_3| \leqslant 0.5$. For example, if $q \leqslant 1$ and $q \leqslant q_l$, then we derive from (3.6) and our last estimates that $\nu(2) \approx 0.25$ and $\nu(3) \approx 0.32$, which would lead us to expect $V(1, 1)$ convergence factors of about 0.063. However, the terms we have neglected in the analysis play a role nar the singularities. For example, for $r = h_r$ and $\Theta = (\pi/2, 0, 0)$ we obtain $A_1 = \frac{4}{5}i$ and $\sqrt[\nu]{|A_1^{2\nu-1}(1-A_1)|/2} = 0.57...$ for $\nu = 2$. This means that the global smoothing factor of this relaxation is at least 0.57 and that we actually could not expect $V(1, 1)$ convergence factors better than 0.3. Nevertheless, the simplifications we made in the analysis are only unreasonable for points lying one or two grid lines away from the singularities. Consequently, the regions where these poorer smoothing factors are achieved are indeed very small and will get increasingly smaller with refinement of the grid. In case these local factors really influence the results, there is always the possibility of applying a few local smoothing sweeps (at low cost, since they are local), then obtaining convergence factors corresponding to the smoothing factors in the main part of the domain, as argued by Brandt [7]. However, in our numerical results we do not observe any significant influence of these locally worse smoothing factors, and consequently, no local sweeps of relaxation are actually required.

### 3.4. *Practical Implementation of Plane Relaxations*; *First Numerical Examples*

We begin by considering examples where the mesh size relations are $q_l = 1$ and $q = \pi/4$. In this case the computational grid is almost uniform (all mesh sizes are similar) and we can expect a good performance by use of $(\phi, \theta)$-plane relaxation. Figure 4 gives a representation through contour lines of the local smoothing factors of plane relaxations. A numerical evaluation of these factors was performed, without making any simplification in the formulas (3.8)–(3.10). Since the coef-

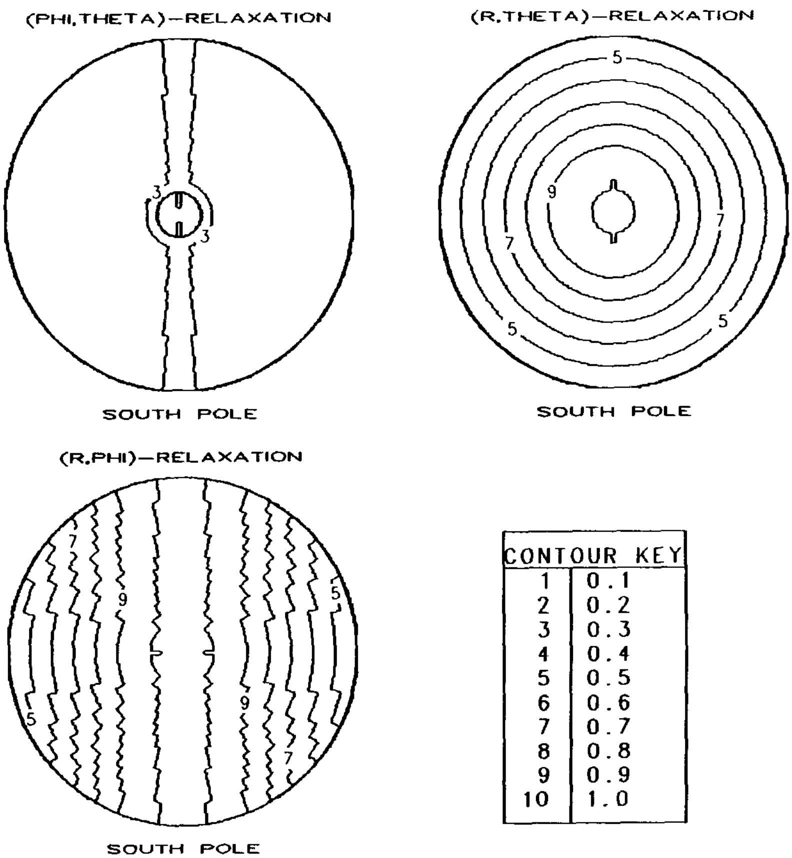


| CONTOUR KEY | |
|---|---|
| 1 | 0.1 |
| 2 | 0.2 |
| 3 | 0.3 |
| 4 | 0.4 |
| 5 | 0.5 |
| 6 | 0.6 |
| 7 | 0.7 |
| 8 | 0.8 |
| 9 | 0.9 |
| 10 | 1.0 |

FIG. 4. Representation of the smoothing factors (with $\nu = 2$) of zebra plane relaxation in different directions for a $16 \times 64 \times 128$ grid with mesh size ratios $q = \pi/4$ and $q_l = 1$.

ficients of the Laplacian do not depend on the $\theta$ variable, it is possible to give a representation of all local smoothing factors in a two-dimensional picture. The full three-dimensional representation would be obtained by rotating the given picture around the pole axis. It can be seen that the factors for the $(\phi, \theta)$-relaxation lie between 0.2 and 0.3 almost everywhere, with the exception of a neighbourhood of the origin where they become slightly worse, as already discussed in the last section. The smoothing properties of the other relaxations are very poor. In most of the domain they lie above 0.7 (everywhere above 0.4) and approach unity near the origin. Before we present numerical results for the current example, we briefly describe the implementation of the plane relaxations. We begin with

• *$(\phi, \theta)$-zebra plane relaxations.* Each $(\phi, \theta)$-plane in the compuational domain (including all grid points for a fixed value of $r$) corresponds to a spherical surface on the physical domain. The discrete two-dimensional problem that has to be solved on each plane is a (discretized) Helmholtz equation, with the Helmholtz coefficient determined by the radial coefficients of the 3D Laplacian and consequently varying from plane to plane. These Helmholtz coefficients are relatively small since the couplings of the 3D-operator in the other directions are strongly dominant (which is actually the reason for needing this plane relaxation). The Helmholtz equation on each plane is approximately solved with the aid of the multigrid solver developed in Section 2. Actually, as also observed in [15], just a rough solution of the equation is needed, a $V(1,0)$-cycle or a $V(1,1)$-cycle of the 2D multigrid solver will be sufficient. The plane relaxation is performed zebrawise, first at odd planes (including the origin and the boundary) and then at even planes. The origin is actually a degenerated plane (for $r=0$) and solving simultaneously for all equations there simply means the solution of Eq. (1.10) for the value at the origin.

• *$(r, \theta)$-zebra plane relaxation.* Each $(r, \theta)$-plane ($\phi$ fixed) corresponds to a conical surface on the physical domain. We again need to solve a Helmholtz equation on each of these planes, with Helmholtz coefficients which depend on $\phi$. The equations are solved by one cycle of a multigrid method, whose components are as follows: It employs combined relaxation, with $\theta$-line relaxation where $qr \leqslant q_l/\sin\phi$ and $r$-line relaxation elsewhere. The method uses standard coarsening, bilinear interpolation as a coarse-to-fine operator, and full-weighting as the fine-to-coarse operator.

For the values $\phi=0$ and $\phi=\pi$ the planes degenerate to a radial line and the simultaneous solution for all unknowns leads to a tridiagonal system, solved by Gauss elimination. The equation at the origin is relaxed separately and the value there is used as a Dirichlet boundary condition for the problems on each plane.

• *$(r, \phi)$-zebra plane relaxation.* The planes now correspond to half discs in the physical domain. The multigrid solver, used in the approximate solution of the corresponding Helmholtz equations for each plane, is based again on standard coarsening, bilinear interpolation, full-weighting, and combined relaxation, which now employs $\phi$-line relaxation where $qr \leqslant 1$ and $r$-line relaxation elsewhere. The

TABLE X

3D $V(1, 1)$ Convergence Factors on a $16 \times 64 \times 128$ Grid with Different Relaxations

| Relaxation | Point red–black | $\theta$-line | $\phi$-line | $r$-line | $r\phi\theta$ altern. line |
|---|---|---|---|---|---|
| Conv. factors | 0.98 | 0.98 | 0.98 | 0.98 | 0.95 |
| CPU (s/cycle) | 1.14 | 1.45 | 1.72 | 1.42 | 3.68 |

*Note.* CPU times per multigrid cycle are given in seconds.

values at the singular axis are relaxed separately and are used as Dirichlet boundary conditions in each plane relaxation.

We come now to the presentation of numerical results. Tables X and XI contains numerically computed asymptotic $V(1, 1)$ convergence factors based on the use of several relaxations. Within each sweep of plane relaxation, one $V(1, 0)$ or $V(1, 1)$ cycle of the 2D multigrid methods is applied on each plane. All results are for the case $q = \pi/4$ and $q_l = 1$, here represented by a $16 \times 64 \times 128$ grid.

The experiments clearly show that relaxations of the wrong type or in the wrong directions produce results that lie far away from those which can be achieved by the [illegible] tions and plane relaxations in the wrong directions produce very poor results. Taking the plane relaxation in the correct direction produces a qualitative improvement. We can also see that one 2D $V(1, 1)$-cycle inside the plane relaxation is enough for good smoothing effects; in fact, nothing further is to be gained by exact solution of the two-dimensional equations. By considering the computational costs, one would even prefer to use the 2D $V(1, 0)$-cycles, which already give very good convergence factors. We remark that the differences in computational costs among the various line and plane relaxations are mainly due to the arrangement of the computational data on the computer. Some line relaxations require much more paging than others. One final remark is that a multigrid cycle with plane relaxation is actually cheaper than one that uses alternating line relaxation.

TABLE XI

3D $V(1, 1)$ Convergence Factors on a $16 \times 64 \times 128$ Grid with Zebra Plane Relaxations

| | Relaxation | | |
|---|---|---|---|
| 2D Cycle-type | $(\phi, \theta)$-plane | $(r, \theta)$-plane | $(r, \phi)$-plane |
| $V(1, 0)$ | 0.115 (2.56) | 0.98 (3.21) | 0.95 (2.87) |
| $V(1, 1)$ | 0.073 (3.34) | 0.98 (3.89) | 0.95 (3.63) |
| Exact | 0.072 (—) | — | — |

*Note.* CPU times per multigrid cycle (in parenthesis) are given in seconds.

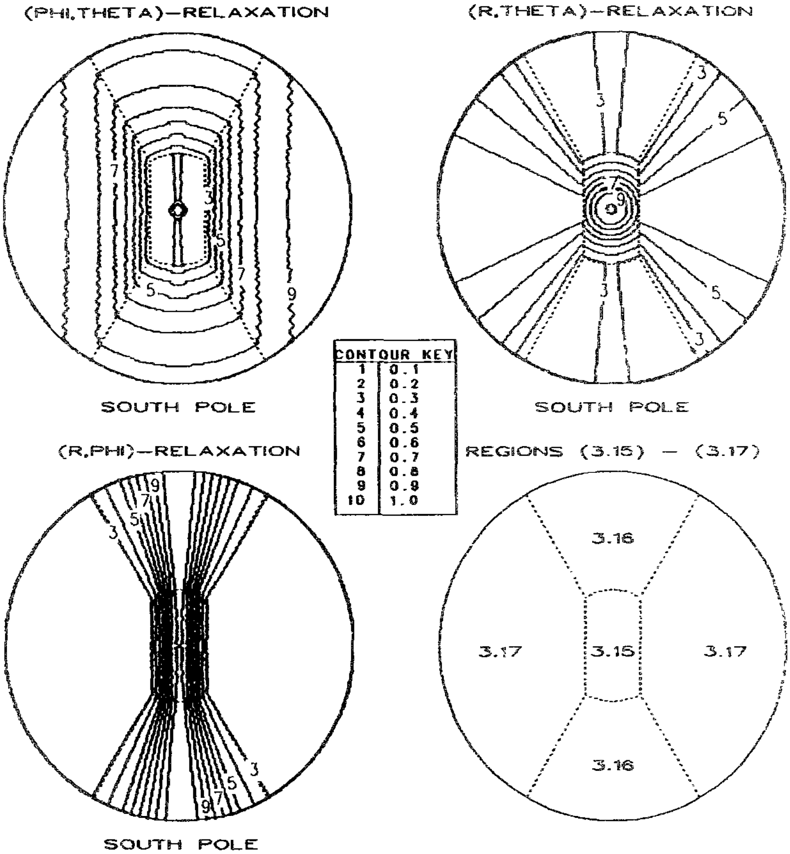


FIG. 5. Representation of the smoothing factors (with $\nu = 2$) of zebra plane relaxation in different directions for a $64 \times 64 \times 64$ grid with mesh size ratios $q = \pi$ and $q_l = 0.5$.

### 3.5. *A More Complex Example; Combined Relaxation in 3D*

The grid used in the example of the last section was in accord with the hypothesis we made, $q \leqslant 1$, $q \leqslant q_l$, when deriving the good smoothing properties for the $(\phi, \theta)$-plane relaxation. Consider now a $64 \times 64 \times 64$ grid, for which $q = \pi$ and $q_l = 0.5$. Figure 5, which presents the smoothing factors of the three plane relaxations in this case, shows that the situation is now completely different. We can see that none of the considered relaxations provides good smoothing overall, their smoothing factors approach unity in some region of the domain. Before analyzing the situation closer, we present numerical experiments with the multigrid method in this case. Tables XII–XIV show convergence factors under use of several relaxation methods.

The numerical results confirm the smoothing analysis; none of the plane relaxations alone produces good convergence factors. Even the combination of plane relaxations in two directions is not enough, only with the alternating plane relaxa-

TABLE XII

3D $V(1, 1)$ Convergence Factors on a $64 \times 64 \times 64$ Grid with Different Relaxations

| Relaxation | Point Red–black | $\theta$-line | $\phi$-line | $r$-line | $r\phi\theta$ altern. line |
|---|---|---|---|---|---|
| Conv. factors | 0.96 | 0.96 | 0.95 | 0.95 | 0.93 |

TABLE XIII

3D $V(1, 1)$ Convergence Factors on a $64 \times 64 \times 64$ Grid with Zebra Plane Relaxations

| | Relaxation | | |
|---|---|---|---|
| 2D cycle-type | $(\phi, \theta)$-plane | $(r, \theta)$-plane | $(r, \phi)$-plane |
| $V(1, 0)$ | 0.88 | 0.95 | 0.95 |
| $V(1, 1)$ | 0.62 | 0.93 | 0.94 |

TABLE XIV

3D $V(1, 1)$ Convergence Factors on a $64 \times 64 \times 64$ Grid with Alternating Zebra Plane Relaxations

| | Altern. plane relaxation | | | |
|---|---|---|---|---|
| 2D cycle-type | $(\phi, \theta)-(r, \phi)$ | $(\phi, \theta)-(r, \theta)$ | $(r, \theta)-(r, \phi)$ | $(\phi, \theta)-(r, \theta)-(r, \phi)$ |
| $V(1, 0)$ | 0.52 | 0.36 | 0.93 | 0.034 |
| $V(1, 1)$ | 0.47 | 0.36 | 0.91 | 0.039 |

tion in all directions are very good convergence factors obtained. This relaxation is, however, very expensive, which motivates the search for more efficient alternatives. In order to be able to reduce the computational costs (and still obtain good convergence), we need to analyze more closely the smoothing factors.

Proceeding as in Section 3.2 (through neglecting the imaginary terms—of first order—in (3.8)–(3.10)) and making some simplifications, we can determine the regions where each plane relaxation smooths very well (with $\mu(2)$ around 0.3). These regions are

*for the $(\phi, \theta)$-plane relaxation*, where

$$qr \leqslant q_l/\sin\phi \quad \text{and} \quad qr \leqslant 1; \tag{3.15}$$

*for the $(r, \theta)$-plane relaxation*, where

$$q_l/\sin\phi \geqslant 1 \quad \text{and} \quad qr > 1; \tag{3.16}$$

*and for the $(r, \phi)$-plane relaxation*, where

$$q_l/\sin\phi < 1 \quad \text{and} \quad qr > q_l \sin\phi. \tag{3.17}$$

These regions are depicted in Fig. 5 (for the $64 \times 64 \times 64$ grid), where we can also see that we have used reasonable approximations when deriving (3.15)–(3.17).

Ideally, we would now subdivide the domain according to (3.15)–(3.17), and restrict the application of each plane relaxation to the corresponding domain where it smooths well. This is, however, not simple to implement.

Initially we will propose a first step in this direction by using a very simple modification of the alternating plane relaxation, which nevertheless reduces the computational work and still provides very good convergence factors. (This is a direct extension to three dimensions of a technique we have used in [2], cf. the remark at the end of Section 2.1.) The idea is to restrict the application of each of the plane relaxations to planes where they give a good smoothing, at least in part of it, according to (3.15)–(3.17). We will clarify this idea for the present example (with $q=\pi$ and $q_l=0.5$). A sweep of the modified alternating plane relaxation (MPR) will comprise:

- $(\phi, \theta)$-plane relaxation only for planes with $r \leqslant 1/\pi$;
- $(r, \theta)$-plane relaxation only for planes with $\sin \phi \leqslant \frac{1}{2}$;
- $(r, \phi)$-plane relaxation everywhere.

With this modification we reduce the total computational work (in the example we are considering) by about 35% and obtain $V(1, 1)$ convergence factors of 0.081. These are still very good, although worse than those obtained with the full alternating plane relaxation. Actually, there is no need for extremely fast convergence factors, since values around 0.1 are all that is needed for solving the equations with FMG (with only one cycle at each level) to the level of truncation errors. Besides that, if we consider the computational work, we see that the MPR relaxation has a better performance than the alternating plane relaxation (see Tables XV and XVI).

However, we have still not achieved a full extension of the combined relaxation, since the relaxations still have a high overlap. For example, the $(r, \phi)$-plane relaxation was applied in the whole sphere, although it is needed only in region (3.17). Its application to all planes cannot, however, be avoided, since this relaxation is

TABLE XV

3D $V(1, 1)$ Convergence Factors on a $64 \times 64 \times 64$ Grid with Alternating Zebra Plane Relaxation, with Modified Alternating Plane Relaxation (MPR) and with Combined Relaxation (COR)

| 2D cycle | Relaxation | Altern. plane | MPR | COR |
|---|---|---|---|---|
| $V(1, 0)$ | Conv. factors | 0.034 | 0.081 | 0.083 |
| | CPU (s/cycle) | 15.22 | 9.77 | 6.99 |
| $V(1, 1)$ | Conv. factors | 0.039 | 0.081 | 0.090 |
| | CPU (s/cycle) | 19.84 | 13.10 | 8.72 |

*Note.* CPU-times per cycle are given in seconds.

TABLE XVI

3D $V(1, 1)$ Convergence Factors per Comparative Work Unit (CWU) on a $64 \times 64 \times 64$ Grid with Alternating Zebra Plane Relaxation, with Modified Alternating Plane Relaxation (MPR), and with combined relaxation (COR)

| Relaxation | Altern. plane | MPR | COR |
|---|---|---|---|
| 2D $V(1, 0)$ | 0.212 | 0.166 | 0.083 |
| 2D $V(1, 1)$ | 0.240 | 0.188 | 0.090 |

responsible for the smoothing in a part of each plane. What we need to do is to restrict the size of each plane. In this way, we will save work not by treating fewer planes, but smaller planes (with fewer unknowns).

The problems related to restricting the size of these planes are that the restriction given by (3.17) is not logically rectangular (a rectangle in the computational domain) and that the number of grid points in each direction after the restriction may not be adequate for coarsening (which normally requires numbers related to powers of two). The solution we propose is to aproximate the restricted region one would like to use by a logically rectangular region such that it contains the restricted region and it is suitable for coarsening.

Before giving a general description of this technique, let us illustrate it for the $(r, \phi)$-plane relaxation in the present example. According to (3.17) we would ideally restrict the relaxation on each plane to the region where $\sin\phi \geqslant \frac{1}{2}$ and $r \geqslant (2\pi \sin\phi)$. The smallest rectangle containing this region is $R = \{(\phi, \theta) \in [\pi/6, 5\pi/6] \times [1/2\pi, 1]\}$. We substitute for $R$ the rectangle $\bar{R} = \{(\phi, \theta) \in [\pi/8, 7\pi/8] \times [\frac{1}{8}, 1]\}$, [illegible] problems on the restricted regions $\bar{R}$, the values at the computational boundary (except at points which lie on the physical boundary) are taken as Dirichlet boundary conditions.

We describe now the extension of the combined relaxation to a general case. It comprises the following steps:

- $(\phi, \theta)$-plane relaxation only for planes with $r \leqslant 1/q$.
- $(r, \theta)$-plane relaxation only for planes with $\sin\phi \leqslant q_l$ (only if region (3.16) is nonempty). On each plane it is restricted to $\bar{R} = \{(r, \theta) \in [a, 1] \times [0, 2\pi]\}$, with $a = b/8$, $b$ the largest integer such that $a \leqslant 1/q$.
- $(r, \phi)$-plane relaxation in all planes (only if region (3.17) is nonempty). On each plane it is restricted to $\bar{R} = \{(r, \phi) \in [c, 1] \times [e\pi, (1-e)\pi]\}$, with $c = d/8$, $c \leqslant q_l/q$, $e = f/16$, $e \leqslant \arcsin q_l$, and the integers $d$ and $f$ taken as large as possible.

These new modifications bring an extra saving of about 30% in the computational costs in relation to the modified plane relaxation and essentially do not

TABLE XVII

3D $V(1,1)$ Convergence Factors with Combined (Plane) Relaxation (Using One 2D $V(1,0)$-Cycle on Each Plane)

| $q$ | $q_l \rightarrow$ | 0.25 | 0.5 | 1.0 | 2.0 |
|---|---|---|---|---|---|
| $\pi/8$ | Grid | $16 \times 128 \times 64$ | $16 \times 128 \times 128$ | $8 \times 64 \times 128$ | $8 \times 64 \times 256$ |
| | | 0.068 | 0.059 | 0.068 | 0.046 |
| | Grid | $8 \times 64 \times 32$ | $8 \times 64 \times 64$ | $4 \times 32 \times 64$ | $4 \times 32 \times 128$ |
| | | 0.064 | 0.056 | 0.061 | 0.043 |
| $\pi/4$ | Grid | $32 \times 128 \times 64$ | $16 \times 64 \times 64$ | $16 \times 64 \times 128$ | $16 \times 64 \times 256$ |
| | | 0.059 | 0.072 | 0.115 | 0.059 |
| | Grid | $16 \times 64 \times 32$ | $8 \times 32 \times 32$ | $8 \times 32 \times 64$ | $8 \times 32 \times 128$ |
| | | 0.046 | 0.069 | 0.100 | 0.056 |
| $\pi/2$ | Grid | $32 \times 64 \times 32$ | $32 \times 64 \times 64$ | $32 \times 64 \times 128$ | $16 \times 32 \times 128$ |
| | | 0.087 | 0.097 | 0.141 | 0.065 |
| | Grid | $16 \times 32 \times 16$ | $16 \times 32 \times 32$ | $16 \times 32 \times 64$ | $8 \times 16 \times 64$ |
| | | 0.072 | 0.087 | 0.123 | 0.061 |
| $\pi$ | Grid | $64 \times 32 \times 32$ | $64 \times 64 \times 64$ | $32 \times 32 \times 64$ | $32 \times 32 \times 128$ |
| | | 0.075 | 0.083 | 0.087 | 0.063 |
| | Grid | $32 \times 32 \times 16$ | $32 \times 32 \times 32$ | $16 \times 16 \times 32$ | $16 \times 16 \times 64$ |
| | | 0.058 | 0.065 | 0.078 | 0.045 |

change the convergence factors. Table XV gives convergence factors ($\rho$) and CPU times with the use of these relaxations. To enable direct comparison between the three relaxation strategies, we define CPU times for the multigrid method with combined relaxation as a "comparative work unit" (CWU) and calculate the convergence factors per CWU ($\rho^{1/\mathrm{CWU}}$), given in Table XVI.

Combined relaxation has made possible a saving of about 55% in computing time in comparison to the alternating plane relaxation, while still furnishing very good convergence factors. The amount of economy it brings depends, of course, on the particular grid being considered (for grids requiring plane relaxation in only one direction, it actually coincides with this relaxation). Nevertheless, it has proved to be very efficient in several different situations. A collection of representative results is presented in the next section.

### 3.6. *Further Numerical Examples; Full Multigrid Results*

Table XVII contains a set of numerical experiments on several grid types. [redacted] $h$-independence for multigrid methods can be observed. More experiments, including tests with Dirichlet boundary conditions and solution of the equation on a spherical gap, can be found in [3].

Table XVIII contains results related to the solution of the Poisson equation with Neumann boundary conditions and an enforced solution equal to $\sin x \sin y \sin 5z$.

TABLE XVIII

Full Multigrid Results for an Exact Solution $\sin x \sin y \sin 5z$

| Grid | Exact error | | FMG error | | CPU ($s$) | Error reduction | |
|---|---|---|---|---|---|---|---|
| | $\| \|_\infty$ | $\| \|_2$ | $\| \|_\infty$ | $\| \|_2$ | | $\| \|_\infty$ | $\| \|_2$ |
| $16\times16\times16$ | 2.18-02 | 3.88-03 | 2.17-02 | 3.79-03 | 0.39 | — | — |
| $32\times32\times32$ | 5.44-03 | 8.95-04 | 5.07-03 | 8.49-04 | 1.52 | 4.01 | 4.34 |
| $64\times64\times64$ | 1.37-03 | 2.17-04 | 1.22-03 | 1.97-04 | 8.84 | 3.97 | 4.12 |
| $8\times16\times32$ | 2.11-02 | 3.94-03 | 2.07-02 | 3.86-03 | 0.31 | — | — |
| $16\times32\times64$ | 5.12-03 | 8.66-04 | 5.22-03 | 8.93-04 | 1.21 | 4.12 | 4.55 |
| $32\times64\times128$ | 1.29-03 | 2.05-04 | 1.41-03 | 2.23-04 | 7.04 | 3.97 | 4.22 |
| $4\times16\times32$ | 2.58-02 | 6.85-03 | 2.58-02 | 6.86-03 | 0.16 | — | — |
| $8\times32\times64$ | 7.06-03 | 1.39-03 | 6.69-03 | 1.30-03 | 0.57 | 3.65 | 4.93 |
| $16\times64\times128$ | 1.81-03 | 3.08-04 | 1.72-03 | 2.95-04 | 3.30 | 3.90 | 4.51 |
| $8\times8\times32$ | 5.53-02 | 1.44-02 | 5.53-02 | 1.44-02 | 0.21 | — | — |
| $16\times16\times64$ | 1.92-02 | 3.32-03 | 1.94-02 | 3.21-03 | 0.69 | 2.88 | 4.34 |
| $32\times32\times128$ | 4.63-03 | 7.64-04 | 4.61-03 | 7.66-04 | 3.73 | 4.15 | 4.35 |
| $8\times16\times16$ | 2.32-02 | 4.34-03 | 2.25-02 | 4.15-03 | 0.28 | — | — |
| $16\times32\times32$ | 5.77-03 | 9.59-04 | 5.44-03 | 9.33-04 | 0.96 | 4.02 | 4.53 |
| $32\times64\times64$ | 1.44-03 | 2.27-04 | 1.31-03 | 2.16-04 | 4.95 | 4.01 | 4.22 |

We used a full multigrid procedure with just one 3D $V(1, 1)$-cycle on each grid level for the solution of the equation to within truncation errors. Tricubic interpolation is used in FMG to transfer solutions from coarser to finer levels. Combined relaxation (with 2D $V(1, 0)$-cycles) is employed in all tests. The results comprise five different grid types, with three grids in each class. The exact discretization errors and the FMG errors (errors in relation to the exact solution after performing the FMG algorithm) are calculated in the uniform and in $L_2$ norm. Error reduction factors (for refinements of the grids within each grid class) are given; they confirm the second order of the discretization. CPU times (in seconds) expended in the solution of the equations are also included.

From the computational costs we can derive some conclusions on the efficiency of the three-dimensional multigrid solver. The solution of the two-dimensional Poisson equation (in Section 2) on a $256\times128$ grid required 0.453 s, while here we need 3.3 s for a solution on a (four times larger) $16\times64\times128$ grid. Using the linear complexity of multigrid solvers, we can estimate that our 2D multigrid solver would require 1.8 s for a solution on a grid of comparable size. This means that the three-dimensional solver (which employs plane relaxations, with line relaxations within them) is less than two times more expensive than the 2D solvers (which in turn are competitive with fast direct solvers). To make a fairer comparison, however, we should take into account that in three dimensions we deal with 7-point stars, in two dimensions only with 5-point stars. We should actually use a multiplicative factor of 7/5 in the estimations for the computing times for the 2D solver, which then lead to an estimate of 2.5 s to solve the equations. The extra costs required by the 3D solver now amount to only about a 30% increase. This is valid for examples which require plane relaxation in only one direction. Consider now the $64 \times 64 \times 64$ grid, with twice the number of grid points and a much more complicated anisotropy pattern. The estimations of computing time for the two-dimensional solver lead now to 5 s, while we actually need 8.84 s with the 3D solver, representing 75% more work. This corresponds roughly to the extra cost of using alternating line relaxations instead of a single line relaxation in two-dimensional problems. The conclusion is that, even in this rather involved case, the three-dimensional solver (with combined relaxation) achieves an efficiency comparable to that of two-dimensional multigrid solvers employing alternating line relaxations.

### 3.7. *Semi-coarsening Strategies*

For problems requiring plane relaxation in connection with standard coarsening, semi-coarsening strategies offer an interesting alternative (e.g., [7]), an alternative which may be simpler and even more efficient. The idea behind semi-coarsening is simple: if a given relaxation does not smooth well in a certain direction, coarsening in this direction should be avoided. In this way, it becomes unnecessary to smooth the error in this particular direction and the given relaxation is made suitable for providing an effective multigrid method. This idea is especially attractive because it may, in principle, make plane relaxation unnecessary.

However, when the anisotropy changes its direction inside the domain, the application of semi-coarsening as a substitute for plane relaxation is nontrivial. In this case, different coarsening directions should be employed in different parts of the domain (according to local anisotropies), leading to complicated grid structures. The resulting schemes would resemble algebraic multigrid schemes (e.g. [12]). One can, instead, employ semi-coarsening as a complement to plane relaxation [8, 9]. The idea then is to coarsen the grid only in one direction and apply plane relaxation on the perpendicular directions, with the goal of obtaining a robust and efficient method (cf. [9]). We feel, however, that neither of these approaches would improve the results obtained with combined relaxation.

In fact, we have compared our multigrid method with the algebraic multigrid solver AMG01 (a solver for symmetric positive definite problems, see [12]), and our solver proved to be faster. For example, a $V(1, 1)$-cycle of our scheme on a $16 \times 16 \times 16$ grid (which leads to a complex anisotropy pattern) takes 0.22 CPU seconds and has a convergence factor of 0.066. The same numbers for AMG01 are: 0.39 CPU seconds (precomputational costs not included) and a convergence factor of 0.18. Similar results were obtained for other mesh size ratios (see [3]). Concerning the method proposed in [9] we can obtain rough estimates by considering operation counts. We compare the number (say $k$) of multiplications/divisions per grid point performed in one FMG-algorithm (with one $V(1, 1)$-cycle on each grid level) for both methods. For grids with varying anisotropy direction (with $q = \pi$, $q_l = 0.5$) we have $k \approx 80$ for our scheme. This value of $k$ reduces to 62 for constant anisotropy direction. The number $k$ given in [9] is 366 (setup costs excluded). We should, however, point out that the algorithm in [9] employs Galerkin operators, which could be avoided for the problems considered here. A more conclusive statement would require further investigation.

In the following, we restrict ourselves to cases with constant anisotropy direction and investigate how semi-coarsening could improve our results. As an example, we take grids with $q=\pi/4$ and $q_l=1$ (as in Section 3.2). In this case, we have seen that using standard coarsening requires plane relaxation in just one direction; we are essentially dealing with the last model case from Table IX. From the model problem analysis we would derive that $\theta$-line relaxation together with $(\phi, \theta)$-semi-coarsening (mesh sizes are doubled in the $\theta$ and $\phi$ directions, but kept constant in the radial direction) is an appropriate combination. A local mode analysis brings further insight. For the mentioned relaxation and semi-coarsening we obtain

$$\mu(v, p) = \sup_{-\pi/2 < \Theta \leqslant \pi/2} \left\{ \sqrt[v]{\frac{|A_1^{2v-1}(1-A_1)|}{2}}, |A_2|^2, \sqrt[v]{\frac{|A_3^{2v-1}(1+A_3)|}{2}}, |A_4|^2 \right\}, \qquad (3.18)$$

with $p \in G_h^{*,0}$ and $A_1$ to $A_4$ given by (3.7). The difference between (3.6) and (3.18) is due to the different coarsening strategies applied (see [3]).

We can now derive (making use of some simplifications) that $\theta$-zebra line relaxation smooths well (when using $(\phi, \theta)$-semi-coarsening) in cases where

$$q_l \geqslant 1 \qquad \text{and} \qquad q \leqslant q_l, \qquad (3.19)$$

for which $V(1, 1)$ convergence factors around 0.1 could be expected. Figure 6 shows the smoothing factors (with $v=2$) for a $16 \times 64 \times 128$ grid with mesh sizes satisfying (3.19). These factors lie overall around 0.3. In Table XIX we present numerical results for a multigrid method employing the analyzed combination of line relaxation and semi-coarsening on grids with the same mesh size relations ($q_l=1$, $q=\pi/4$). $V(1, 1)$ convergence factors (together with the number of grid levels employed within the multigrid method) are given.

The results are quite disappointing. While for relatively coarse grids (with just two or three grid levels within the multigrid cycle) there is still a correspondence between predictions and results; we can observe a rapid deterioration of the convergence factors when the grids are refined (and/or more grid levels are used).

TABLE XIX

3D $V(1, 1)$ Convergence Factors with Semi-Coarsening ($q_l=1$, $q=\pi/4$)

| Grid | Grid levels | Convergence factors |
|---|---|---|
| $4 \times 16 \times 32$ | 2 | 0.079 |
| $8 \times 32 \times 64$ | 3 | 0.15 |
| $16 \times 64 \times 128$ | 4 | 0.35 |
| $16 \times 64 \times 128$ | 5 | 0.60 |

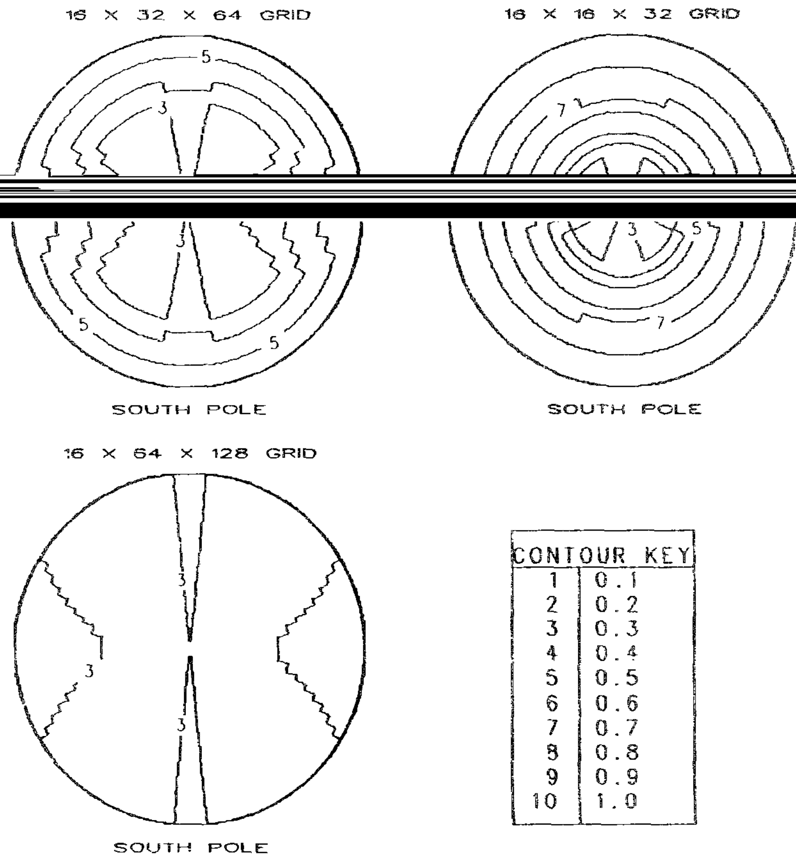


| CONTOUR | KEY |
|---|---|
| 1 | 0.1 |
| 2 | 0.2 |
| 3 | 0.3 |
| 4 | 0.4 |
| 5 | 0.5 |
| 6 | 0.6 |
| 7 | 0.7 |
| 8 | 0.8 |
| 9 | 0.9 |
| 10 | 1.0 |

FIG. 6. Representation of the smoothing factors (with $\nu = 2$) of $\theta$-line relaxation in connection with $(\phi, \theta)$-semi-coarsening in several grids (with different mesh size ratios).

A kind of $h$-dependence is present here and the results seem to contradict the smoothing analysis.

This is, however, not the case. A closer consideration of the smoothing analysis actually explains what occurs here. Figure 6 shows, in addition to the smoothing factors for the $16 \times 64 \times 128$ grid treated in the numerical experiments, the factors for a $16 \times 32 \times 64$ grid (worse) and for a $16 \times 16 \times 32$ grid (considerably worse). It happens that these two other grids are the first two coarser grids for the first one under application of $(\phi, \theta)$-semi-coarsening. The behavior of the anisotropy changes completely when passing to the coarser grids; in particular, it now changes its direction inside the domain, which does not happen on the finest grid. The semi-coarsening produces a modification on the meshsize relation $q$ from $\pi/4$ to $\pi/2$ and then to $\pi$ ($q_l$ remains 1). The combination of $\theta$-line relaxation and $(\phi, \theta)$-semi-coarsening ceases to be adequate on coarser grids.

Semi-coarsening also has the potential to change the anistropy for the model case

$$au_{xx} + bu_{yy} + cu_{zz}, \qquad \text{with} \quad a \ll b \ll c,$$

for which $z$-line relaxation together with $(y, z)$-semi-coarsening is recommended. Each step of the coarsening process causes a relative growth of $a$ by a factor 4, while keeping $b$ and $c$ unchanged. If the number of levels on the multigrid process is large enough, the point will be reached where $a \approx b \ll c$ and for even coarser grids the anisotropy will be qualitatively different from that on the finest grid. There is however a simple way of treating this problem. If we switch to standard coarsening (keeping the same relaxation) when we reach the grid where $a \approx b \ll c$, we will achieve an effective method (since the $z$-line relaxation will smooth well in all directions on this grid and on all coarser ones, where the problem will keep the same features, due to the change to standard coarsening). This combination of line relaxation with semi-coarsening on finer grids and with standard coarsening on coarser grids will not only solve the problem, but it will lead also to a method which is more efficient than one employing standard coarsening and plane relaxation.

The problem we are dealing with is, however, more complicated. When we reach the point (coarser grid) where we should change strategy (actually very soon), we cannot switch to standard coarsening and keep using line relaxation. Already on the first coarse grid, much more accentuated on the second one, the anisotropy has a change of direction inside the domain. The problem to solve on the coarser grid is actually of a more complicated nature (in contrast to the model case) than the problem on the finest grid, since it requires semi-coarsening in more than one direction or, alternatively, plane relaxation in more than one direction. In order to achieve any gain by using semi-coarsening on the first one or two grids (and saving the plane relaxation there), we have to handle these (more complicated) coarse grid problems efficiently, since they actually occur on relatively fine grids.

TABLE XX

3D $V(1, 1)$ Convergence Factors with the Combination of Semi- (on Finer Levels) and Standard (on Coarser Levels) Coarsening

| $q$ | LSC | $q_l \rightarrow$ | 1.0 | 2.0 |
|---|---|---|---|---|
| | | Grid | $16 \times 64 \times 128$ | $16 \times 64 \times 256$ |
| $\pi/4$ | 0 | | 0.115 (2.56) | 0.059 (4.90) |
| | 1 | | 0.114 (2.02) | 0.068 (3.80) |
| | 2 | | 0.179 (1.70) | 0.109 (3.26) |
| | 3 | | 0.35 (1.61) | 0.33 (3.11) |
| | 4 | | 0.60 (1.60) | 0.59 (3.09) |

*Note.* LSC gives the number of finer grids on which semi-coarsening is applied. CPU times per cycle (in parenthesis) are given in seconds.

Fortunately, the multigrid solvers with standard coarsening and the combined relaxation (instead of alternating plane relaxations which would be normally required) give an efficient solution to these coarse grid problems. It is then possible, with a mixed strategy which combines line relaxation and semi-coarsening on the first (one or two) finer grids with standard coarsening and combined relaxation on the remaining coarser grids, to get an improvement in efficiency. This method is about 20 to 30% faster than the multigrid solver with just standard coarsening and plane relaxation and has similar convergence factors. Employing semi-coarsening on even more grid levels causes a deterioration of the convergence factors and is not recommended, as can be seen in Table XX. Numerical results with the use of semi-coarsening on the first one to four grid levels (on the coarser levels we then switch to standard coarsening and combined relaxation) are presented. Results with just standard coarsening (semi-coarsening on the first 0 levels) are given for comparison.

We have seen that semi-coarsening is an interesting option to improve efficiency, at least for problems with constant anisotropy directions. However, it does not in general eliminate the need for plane relaxations.

## 4. Conclusions

This work describes the development of multigrid methods for Poisson- and Helmholtz-type equations on the sphere. The two-dimensional multigrid solvers (for equations on the surface of a sphere) achieve the efficiency of specialised fast direct solvers. Moreover, they present the advantages of better complexity (work proportional to the number of unknowns) and broader applicability (e.g., [5]). The efficiency of this multigrid solver is maintained, even in the presence of varying anisotropy direction. This is possible through the introduction of the new *combined relaxation* method, which replaces the twice more expensive alternating line relaxation.

The strong and varying anisotropy of the equations on the sphere pose difficulties for the realization of efficient three-dimensional multigrid schemes. The use of plane relaxations, implemented with aid of two-dimensional multigrid solvers, is required for achieving an effective method. More complicated anisotropy patterns, which are present for some grid choices, would even require alternating plane relaxations. A detailed local Fourier analysis provides the guide lines to the extension of combined relaxation to three dimensions; with this technique (instead of alternating plane relaxations) the results are highly improved. The 3D solvers achieve an efficiency comparable to that of two-dimensional multigrid schemes (for the solution of problems of comparable difficulty).

The use of semi-coarsening strategies for three-dimensional problems with varying anisotropies is also analyzed. The combination of it with the previously developed techniques can make the solver even faster.

The fast convergence of the multigrid methods ($V(1, 1)$ convergence factors around 0.1 in all cases) is used to obtain a very efficient full multigrid procedure. With just one $V(1, 1)$ multigrid cycle on each grid level (within the FMG) the equations are solved to below the level of the truncation errors.

## Acknowledgments

This work is part of my Ph.D. dissertation [3], presented at the University of Bonn. I thank my thesis advisor, U. Trottenberg, for his excellent guidance and constant support. Numerous other people contributed in one way or another, through fruitful discussions, suggestions, support, and encouragement, to the realization of this work. I would like to mention J. Blatter, A. Brandt, J. Linden, R. Lorentz, K. Stüben, H. Unger, and all of my colleagues from the GMD multigrid group. G. Lonsdale helped a lot by reading and commenting on this paper. Comments from the referees contributed to improve the final form of the manuscript. My sincere thanks to them all.

## References

1. J. Adams, P. Swarztrauber, and R. Sweet, NCAR, Boulder, CO 80307, 1979 (unpublished).
2. S. R. M. Barros, *Appl. Math. Comput.* **25**, 123 (1988).
3. S. R. M. Barros, *Optimierte Mehrgitterverfahren für zwei- und dreidimensionale elliptische Randwertaufgaben in Kugelkoordinaten*, Dissertation, Universität Bonn, 1988. GMD-Bericht 178 (Oldenbourg Verlag, München/Wien, 1989).
4. S. R. M. Barros, D. P. Dee, and F. Dickstein, *Atmos. Ocean.* **28**, 24 (1990).
5. J. R. Bates, F. H. M. Semazzi, R. W. Higgins, and S. R. M. Barros, *Mon. Wea. Rev.* **118**, 1615 (1990).
6. A. Brandt, *Math. Comput.* **31**, 333 (1977).
7. A. Brandt, *Multigrid Techniques*: 1984 *Guide with Applications to Fluid Dynamics* (GMD Studie 85, St. Augustin, 1984).
8. N. Decker and J. V. Rosendale, in *Proceedings, Fourth Copper Mountain Conference on Multigrid Methods*, edited by J. Mandel *et al.* (SIAM, Philadelphia, 1989).
9. J. E. Dendy, Jr., S. F. McCormick, J. W. Ruge, T. F. Russel, and S. Schaffer, "Multigrid Methods for Three-Dimensional Petroleem Reservoir Simulation," SPE Paper 18409, Symposium on Reservoir Simulation, Houston, TX, February 6–8, 1989.
10. W. Hackbush, *Multigrid Methods and Applications* (Springer-Verlag, Berlin, 1985).
11. J. Linden, U. Trottenberg, and K. Witsch, in *Proceedings, 4th GAMM-Conference on Numerical Methods in Fluids Dinamics*, edited by H. Viviand (Wieweg, Braunschweig, 1982).
12. J. Ruge and K. Stüben, in *The Institute of Mathematics and its Applications Conference Series, New* [illegible]
W. Hackbusch and U. Trottenberg, Lect. Notes in Math., Vol. 960 (Springer-Verlag, Berlin, 1982).
14. P. Swarztrauber, *J. Comput. Phys.* **15**, 46 (1974).
15. C. Thole and U. Trottengerg, in *Notes on Numerical Fluid Mechanics*, Vol. 11, edited by D. Braess *et al.* (Vieweg, Braunschweig, 1985).